Bloch Oscillations of THz Acoustic Phonons in Coupled Nanocavity Structures

N. D. Lanzillotti-Kimura,[1,2,*] A. Fainstein,[1] B. Perrin,[2] B. Jusserand,[2] O. Mauguin,[3] L. Largeau,[3] and A. Lemaître[3]

[1]*Centro Atómico Bariloche and Instituto Balseiro, C.N.E.A., R8402AGP S. C. de Bariloche, Río Negro, Argentina*

[2]*Institut des Nanosciences de Paris, UMR 7588 C.N.R.S.—Université Paris 6, 74015 Paris, France*

[3]*Laboratoire de Photonique et de Nanostructures, C.N.R.S., Route de Nozay, 91460 Marcoussis, France*

(Received 14 December 2009; revised manuscript received 22 March 2010; published 13 May 2010)

Nanophononic Bloch oscillations and Wannier-Stark ladders have been recently predicted to exist in specifically tailored structures formed by coupled nanocavities. Using pump-probe coherent phonon generation techniques we demonstrate that Bloch oscillations of terahertz acoustic phonons can be directly generated and probed in these complex nanostructures. In addition, by Fourier transforming the time traces we had access to the proper eigenmodes in the frequency domain, thus evidencing the related Wannier-Stark ladder. The observed Bloch oscillation dynamics are compared with simulations based on a model description of the coherent phonon generation and photoelastic detection processes.

DOI: 10.1103/PhysRevLett.104.197402 PACS numbers: 78.67.Pt, 63.22.Np, 78.30.−j, 78.67.De

A homogeneous static electric field applied to a crystal induces an oscillatory motion of the electrons; this constitutes one of the most striking and counterintuitive results of quantum effects in solids: the electronic Bloch oscillations (BOs) [1,2]. This phenomenon was experimentally demonstrated 60 years after the original theoretical prediction, with the advent of semiconductor superlattices [3]. The frequency counterpart of BOs are the Wannier-Stark ladders (WSLs) [4], a series of energy levels separated by a constant value. During the last 15 years BOs and WSLs of atoms [5,6], Bose-Einstein condensates [7], plasmons [8], photons [9,10], and sound [11–13] were also demonstrated proposing alternative ways to mimic the effects of the periodic linear potentials. We have recently predicted the existence of GHz-THz nanophononic BOs and WSLs [14,15] in systems formed by a series of coupled acoustic nanocavities [16,17]. Here, we report the first experimental observation of this phenomenon. By performing coherent acoustic phonon generation experiments [18–22], subterahertz hypersound was generated and detected with light inside the structure. These time resolved experiments allowed us to analyze the acoustic phonon dynamics both in the time and frequency domains.

Each time an electron fulfills the Bragg condition, it gets reflected changing its propagation direction. In the case of electronic BOs this is achieved by accelerating the electrons using the electric field, and thus changing the electron wavelength. An analogue result could be achieved by changing the lattice parameter of the structure as a function of the position, while keeping constant the electron wavelength. Taking advantage of this alternative, it is possible to extend the BO phenomenon to other excitations that do not have an associated canonical potential as would be the electric field for electrons, as is the case of photons and phonons. Nanophononic BOs (NBOs) have been predicted and studied theoretically, but not yet observed experimentally [14,15]. In order to evidence the NBOs, a parallelism between the attractive potential for electrons of single atoms, and the phononic response of planar acoustic nanocavities, can be established [15,16]. The latter confine hypersound both spectrally and spatially. We note that acoustic phonons in nanocavities are confined through weak multiple reflections and interference by distributed Bragg mirrors. In addition, the coherence length of acoustic phonons is much longer than that of electrons. These features make acoustic phonons attractive for the study of BOs at room temperature. In this Letter we present experimental results that evidence the existence of NBOs and WSLs in the THz range. We note that previous experimental results in the study of photonic BOs rely on the tunneling of waves through the structures, and the use of standard transmission experiments [9–13]. In contrast, with the picosecond ultrasonics techniques described here acoustic phonons are both generated and detected with light inside the coupled nanocavity structure, thus bringing a much closer parallel with the phenomena based on electrons.

An acoustic nanocavity consists of two phononic distributed Bragg reflectors (BRs) enclosing a spacer [16,23]. The BRs are formed by a periodic array of bilayers of two materials with different acoustic impedance [24]. The studied structure consists of a series of 15 coupled acoustic nanocavities. A schematic of the sample is shown in Fig. 1. Each unit cell of the superstructure is formed by 6.5 periods of AlAs/GaAs ($\lambda_c/4$, $3\lambda_c/4$) BR, and a GaAs acoustic spacer ($\lambda_c/2$), where λ_c is the acoustic wavelength of the confined cavity mode. Each spacer is thus enclosed by two BRs, one corresponds to the same unit cell, and the other corresponds to the cell immediately to the right. The sample was grown on a (001) GaAs substrate by molecular beam epitaxy, producing sharp and planar interfaces at the atomic level. This is a strong requirement to study the THz phonon dynamics (nm wavelengths). The coupling between the acoustic nanocavities will develop phononic conduction bands and band gaps [15]. In order to mimic the effects of a linear potential, the energy of the ith cavity must differ from that of the $(i-1)$th cavity in a constant

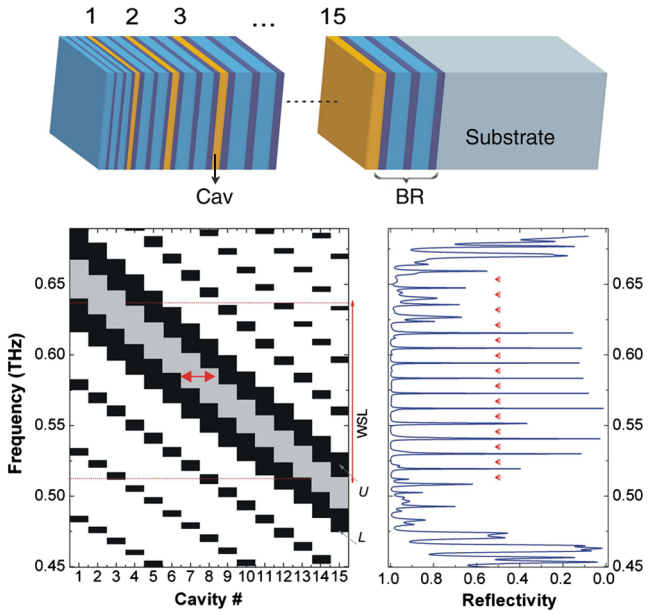

FIG. 1 (color online). Top: Schematic of the coupled nanocavities nanostructure. Bottom left: Phonon band structure. The central grey region (indicated with a double arrow) limited by the thicker black forbidden bands corresponds to the cavity-mode band. L, U, and WSL indicate the lower and upper minigaps, and the acoustic WSL region. Bottom right: Calculated acoustic reflectivity. Red triangles indicate the resonance energies of the isolated nanocavities.

value [14,15]. This is equivalent to linearly modifying the energy levels of the individual atoms in a periodic array, which coincides with the effect of applying a linear electric potential. Such dependence with position of the phonon cavity-mode energy can be obtained by tuning the cavity widths. In our case, a linear shift of 10.8 GHz per cavity was established, being the first cavity energy set at 0.654 THz. This gradient leads to BOs with a period of $\approx$92.6 ps [15], the 15 nanocavities (building blocks) making the structure amount to 209 nanometric layers, with layer thicknesses varying from 2.17 to 7.14 nm. These thicknesses were verified by high resolution x-ray diffraction, and simulations. The latter show an excellent agreement with the experiments using the nominal values and no fitting parameters.

In the left panel of Fig. 1 we present the schematic band structure, calculated as described in Ref. [15]. This phonon band structure represents a practical way to identify the tilted bands and spatial localization of the modes. Black (white) regions represent the phononic band gaps (bands). The central miniband (indicated in grey) arises from the coupling of the individual nanocavities. It is worth noting that without cavity-mode energy shift, this band would be horizontal. We label the enclosing broader minigaps as the lower (L) and upper (U) minigaps. The frequencies for which both minigaps limit the grey nanocavity band determines the region in which the nanowaves are spatially confined, thus leading to the apparition of the WSL energy levels. Acoustic phonons with appropriate energies will bounce back and forth between the lower and upper tilted minigaps. The BO period is determined by the energy gradient imposed on the nanocavity energies: by increasing the gradient, the period will be smaller and the acoustic phonon packet will be more localized in space. The horizontal arrow indicates the confinement region ($\sim$3 spacers) for a given energy. The right panel of Fig. 1 shows the calculated acoustic reflectivity of the structure considering a semi-infinite GaAs medium at both sides of the structure. The high reflectivity band between 0.480 and 0.674 THz is determined by the superposition of the individual stop bands of the unit cells. The equidistant central dips correspond to the phononic WSL. Each nanocavity has an associated resonance frequency determined by its thickness. The red triangles indicate the confined mode frequencies of the isolated nanocavities ($\nu_c = v/\lambda_c$, where v is the sound velocity in the spacer). The coupled states correspond to collective modes of the complete structure. We emphasize that due to the coupling effects the isolated nanocavity frequencies do not match the dips, which reflect the proper modes of the WSL.

In order to evidence the NBOs and WSL, acoustic phonons need to be generated and detected as they interact with the structure. Pump-probe coherent phonon generation experiments [18–22] were performed using a Ti:sapphire laser which delivers 100 fs pulses. The pump pulse impinges the sample generating the acoustic phonons, while the delayed probe pulse senses the optical reflectivity changes. Pump and probe pulses were focused superimposed on a $\sim$50 μm spot, with typical powers of 55 and 10 mW, respectively. The experiments were performed at room temperature and with the laser wavelength set at 815 nm. For this wavelength the laser energy is above the gap, but penetrates the whole structure. A typical time trace is shown in Fig. 2(a). A slowly varying background related to the thermal and electronic responses of the system has been subtracted for clarity. The measured signal starts at $t = 0$ ps with a rapid reflectivity variation, originated by the fast electronic response of the structure. Clear $\sim$22.5 ps period oscillations can be observed. They are related to the Brillouin scattering of propagating acoustic waves both in the nanostructure and the GaAs substrate. By filtering the signal, we can get rid of the low frequency part of the spectrum and analyze the high frequency phonon dynamics. In Fig. 2(b) we show the signal after applying a bandpass filter between 0.517 and 0.636 THz, i.e., covering the region of the WSL. The low frequency oscillations have been eliminated, unmasking a very rich high frequency time trace (see the insets). It is possible to identify beatings in the amplitude of the signal with an approximate period of $\sim$95 ps. As we will show below, this is directly related to the BOs experienced by the hypersound.

As both the generation and the detection of acoustic phonons are distributed over the whole device, by Fourier transforming the time dependent reflectivity signal it is

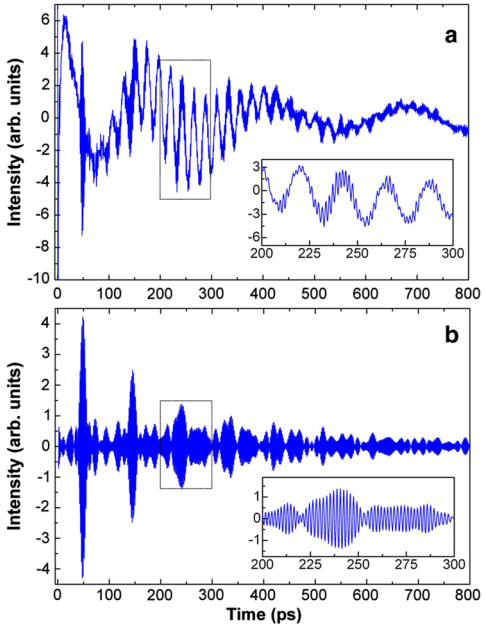

FIG. 2 (color online). Time resolved reflectivity measured on a structure formed by 15 coupled acoustic nanocavities. (a) Measured signal using a laser wavelength of 815 nm without a slowly varying background. (b) Signal after applying a bandpass filter set between 0.517 and 0.636 THz. The insets show a zoom of the time trace between 200 and 300 ps.

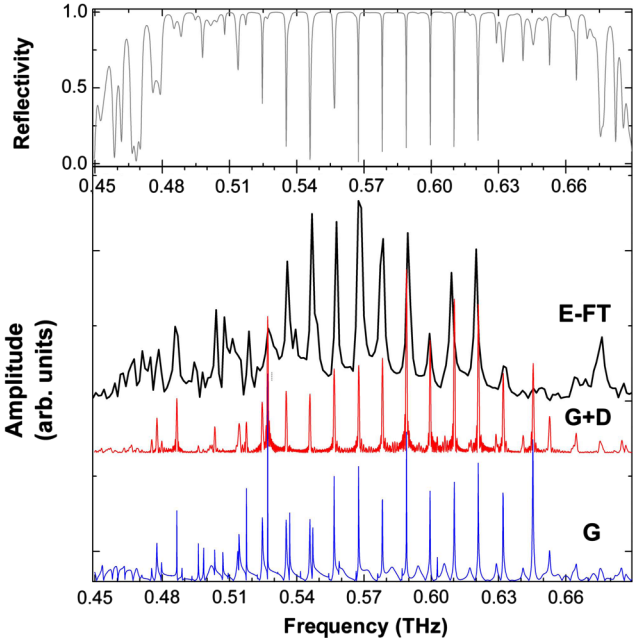

FIG. 3 (color online). Upper panel: calculated acoustic reflectivity of the studied structure. The dips correspond to the nanophononic WSL energy levels. Lower panel: Fourier transform of the derivative of the experimental signal shown in Fig. 2 (*E-FT*), simulated spectrum ($G + D$), and computed acoustic phonon generation spectrum (G).

possible to sense the acoustic eigenstates of the full cavity system. Figure 3 shows the Fourier transform (*E-FT*) of the experimental signal shown in Fig. 2. Notably, it is characterized by a series of equidistant peaks between 0.53 and 0.62 THz, plus some additional features. For clarity reasons, the calculated acoustic reflectivity is also included in the top panel. Note the coincidence between the measured acoustic modes and the dips in the reflectivity corresponding to the phononic WSL, without any fitting parameter in the latter.

We performed numerical simulations using a theoretical model based on a spatially dependent impulsive generation of hypersound, followed by a photoelastic detection process [18,22]. The generated spectrum is calculated assuming that at time zero an ultrafast electromagnetic pulse defines a strain that is distributed along the structure and depends on the material light-sound transduction constant. Since the laser energy is near (far from) the fundamental electronic transition of the GaAs (AlAs) layers, the main contribution to the electron-hole pair generation and photoelastic mechanism will be localized only in the GaAs quantum wells. We thus consider this constant ≈ 0 for AlAs but finite for GaAs. To characterize the detection properties of the device we evaluate the time dependent change in reflectivity induced through a photoelastic mechanism. Standard values for the materials properties were used, without any adjustment parameter [25]. The simulated spectrum ($G + D$) is displayed in Fig. 3. The simulation reproduces all the main features of the experimental spectrum with a remarkable agreement, in particular, the spectral position of the peaks corresponding to the WSL. The theoretical FT was performed over 800 ps to take into account the finite experimental integration time. The spectra differs, however, in the linewidth of the modes. In fact, the simulations do not consider acoustic absorption effects that could be significant at room temperature, electronic resonances with individual quantum wells [26], or light absorption effects. In addition, surface roughness, particularly at the air-sample interface, could lead to an additional broadening mechanism [27]. The generated phonons (shown in Fig. 3, labeled with G) are exactly the same as the ones experiencing the BOs. That is, the phonons do not have to tunnel the band gaps to start oscillating; they are created in the spatial region confined by the tilted upper and lower minigaps, in close analogy with the classical electronic BOs.

One of the most important advantages of the method used to study the NBOs with respect to other techniques is that the time domain information is directly available. In our case, it is possible to filter the signal in order to analyze an individual acoustic wave packet experiencing BOs, isolated from the ensemble of acoustic phonons oscillating within the whole structure. To further understand the nature of the time response of our system, we filtered the measured time trace using a bandpass filter between 0.554 and 0.585 THz. This band comprises three peaks of the phononic WSL, which can be related to specific regions of the sample. In the right panel of Fig. 4 we show the resulting

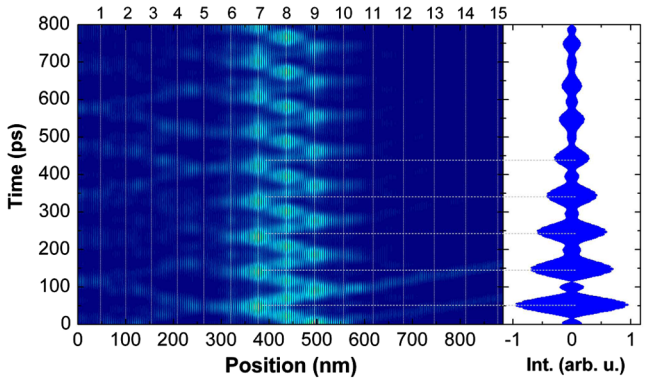

FIG. 4 (color online). Left panel: simulated time evolution of the generated spectrum between 0.554 and 0.585 THz. The white vertical lines indicate the positions of the acoustic spacers. Right panel: experimental signal treated with a bandpass filter between 0.554 and 0.585 THz. Horizontal lines are a guide to the eye to relate the maxima in the detected signal with the localization of maxima of acoustic deformation in the structure.

filtered experimental time trace. Note that oscillations can be clearly observed, and have a very well defined period of 95.3 ps, in agreement with the expected theoretical BO period $\tau = h/\Delta\omega$ of 92.7 ps. These oscillations can be related to the beatings observed in Fig. 2(b). In order to analyze the time dependence of the experimental signal we compare it with the time evolution of the simulated generation spectrum. We computed the time evolution of the simulated generated phonon pulse as

$$u(z, t) = \int_{\omega_1}^{\omega_2} u(z, \omega) e^{-i\omega t} d\omega, \quad (1)$$

where u is the atomic displacement, ω the phonon frequency, and ω_1 and ω_2 are the same limits defined for the filtering of the experimental signal. The $u(z, \omega)$ functions are the set of eigenstates of the elastic equations governing the atomic displacement [15]. $|u(z, t)|^2$ is shown in the left panel of Fig. 4, where clear (dark) zones indicate maxima (minima) in the displacement amplitude. The vertical white lines indicate the position of the acoustic spacers in the structure. Observing the simulations, it is possible to identify the spatial region where the BOs take place. In this particular case, phononic BOs develop between cavities 7 and 9, in agreement with the band structure scheme shown in Fig. 1. By shifting the filter window, the region where BOs developed would also be changed. The horizontal dotted lines in Fig. 4 are a guide to the eye indicating the maxima in the filtered experimental time trace. In this case, comparing the simulations with the experimental time signal it is evident that the detection is maximum when the phonon packet passes through cavity number 7. This can be understood considering that there must be a phase matching between the electromagnetic field, acoustic strain, and photoelastic pattern, which determines which modes are more efficiently detected [22,24]. The result presented in Fig. 4 is consistent with the conceptual design of the sample.

In conclusion, we have experimentally demonstrated NBOs and WSLs in coupled acoustic nanocavity structures, generating and detecting THz acoustic nanowaves using femtosecond laser pulses. The experiments reflect the presence of the proper modes of the artificially engineered phononic potential. Our results constitute a clear example where the capability to generate and detect ultrahigh frequency phonons, and the ability to fabricate samples with specifically engineered nanometric modulations and atomic level interface quality, added to the potentiality to manipulate electronic, magnetic, and optical properties with hypersound open new possibilities in the field of nanophononics.

*kimura@cab.cnea.gov.ar

[1] F. Bloch, Z. Phys. **52**, 555 (1929).
[2] C. Zener, Proc. R. Soc. A **145**, 523 (1934).
[3] C. Waschke *et al.*, Phys. Rev. Lett. **70**, 3319 (1993).
[4] A. G. Chynoweth *et al.*, Phys. Rev. Lett. **5**, 57 (1960).
[5] M. Ben Dahan *et al.*, Phys. Rev. Lett. **76**, 4508 (1996).
[6] Steven R. Wilkinson *et al.*, Nature (London) **387**, 575 (1997).
[7] O. Morsch *et al.*, Phys. Rev. Lett. **87**, 140402 (2001).
[8] Artur R. Davoya *et al.*, Appl. Phys. Lett. **94**, 161 105 (2009).
[9] R. Sapienza *et al.*, Phys. Rev. Lett. **91**, 263902 (2003).
[10] V. Agarwal *et al.*, Phys. Rev. Lett. **92**, 097401 (2004).
[11] Helios Sanchis-Alepuz, Yuriy A. Kosevich, and Jose Sanchez-Dehesa, Phys. Rev. Lett. **98**, 134301 (2007).
[12] Zhaojian He *et al.*, Phys. Rev. E **76**, 056605 (2007).
[13] L. Gutierrez *et al.*, Phys. Rev. Lett. **97**, 114301 (2006).
[14] N. D. Lanzillotti Kimura, A. Fainstein, and B. Jusserand, Phys. Rev. B **71**, 041305(R) (2005).
[15] N. D. Lanzillotti-Kimura *et al.*, Phys. Rev. B **75**, 024301 (2007).
[16] M. Trigo *et al.*, Phys. Rev. Lett. **89**, 227402 (2002).
[17] P. Lacharmoise *et al.*, Appl. Phys. Lett. **84**, 3274 (2004).
[18] C. Thomsen *et al.*, Phys. Rev. B **34**, 4129 (1986).
[19] A. Bartels *et al.*, Appl. Phys. Lett. **72**, 2844 (1998).
[20] K. Mizoguchi *et al.*, Phys. Rev. B **55**, 9336 (1997).
[21] C.-K. Sun, J.-C. Liang, and X.-Y. Yu, Phys. Rev. Lett. **84**, 179 (2000).
[22] N. D. Lanzillotti-Kimura *et al.*, Phys. Rev. Lett. **99**, 217405 (2007).
[23] A. Huynh *et al.*, Phys. Rev. Lett. **97**, 115502 (2006).
[24] B. Jusserand and M. Cardona, in *Light Scattering in Solids V*, edited by M. Cardona and G. Güntherodt (Springer, Heidelberg, 1989).
[25] S. Adachi, J. Appl. Phys. **58**, R1 (1985).
[26] M. F. Pascual Winter *et al.*, Phys. Rev. Lett. **98**, 265501 (2007).
[27] C.-L. Hsieh *et al.*, Appl. Phys. Lett. **85**, 4735 (2004).